C ‹

a

fining walls, we measured the elastic repulsive interactions of these particles with confining surfaces and found that separation-dependent particle–wall interaction force is a non-monotonic function of separation and shows oscillatory behavior. We show that gourd-shaped particles in cholesterics reside not on a single sedimentation level, but on multiple long-lived metastable levels separated by a distance comparable to cholesteric periodicity. Finally, we demonstrate three-dimensional laser tweezers assisted assembly of gourd-shaped particles taking advantage of both orientational order and twist periodicity of cholesterics, potentially allowing new forms of orientationally

laser-tweezers-assisted assembly of gourd-shaped particles using both orientational order and the intrinsic periodicity of CLCs.

Materials and techniques

We used gourd-shaped polystyrene nonspherical colloidal particles with two lobes of dimensions $L_1 \approx 5$ μm and $L_2 \approx 2$ μm on average (Fig. 1a–d), which were synthesized using a modified seeded polymerization technique.[51] To make them responsive to magnetic fields, they were soaked in a toluene dispersion of synthesized $CoFe_2O_4$ ferromagnetic nanoparticles[52] with a mean diameter of 10 nm for ~48 h. Ferromagnetic nanoparticles were trapped in the surface layer of gourd-shaped particles due to partial swelling of polystyrene in toluene. A cholesteric LC with a pitch (distance at which LC molecules or a director $\hat{\mathbf{n}}$ twist by 2π) of $p_0 = 5$ μm was prepared by mixing a nematic material ZLI-3412 and a chiral additive CB15 (both from EM Industries) in weight proportion of

gourd-shaped particles was realized with a holographic optical trapping system[53,55] operating at a wavelength of $\lambda = 1064$ nm

particle around its short axis parallel to $\mathbf{c}$ and translational displacement along $\mathbf{c}$, which we verified below using magnetic manipulation. This coupling allows determination of the vertical displacement of a particle along z-axis using the change of its orientation in the plane of the cell.

Application of a magnetic field $\mathbf{H}$ to the magnetically functionalized gourd-shaped particles results in an induced net magnetic dipole moment $\mathbf{m}$, which allows us to use magnetic manipulation techniques[56] to control the orientation of the particles about all Euler angles (Fig. 3). When magnetically trapped, the orientation of these particles fluctuates with respect to the direction of a maximum accessible applied magnetic field equal to 10.7 mT by an angle $\Delta q \approx \pm 0.86^{\circ}$ (Fig. 3a). The orientational trapping stiffness k_q associated with magnetic trapping can be determined similar to the approach in optical trapping[60] using the equipartition theorem $\langle \Delta q^2 \rangle = k_B T/k_q$, where $\langle \Delta q^2 \rangle$ is a standard deviation in the orientation of a particle with respect to $\mathbf{H}$, k_B is Boltzmann's constant and T is temperature. Fitting the histogram of angular deviations (Fig. 3a) with a function $f(\Delta q) = f_0 \exp[-\Delta q^2/(2\langle \Delta q^2 \rangle)]$, one finds $\langle \Delta q^2 \rangle = 2.25 \times 10^{-4}$ rad^2, which yields $k_q = 18.39$ pN μm. The

force can be neglected in the case of thin LC cells as it is one-to-three orders of magnitude smaller as compared to the maximum elastic force (Fig. 4h and k). Magnetic manipulation is working against the repulsive force F_w when moving the particle towards the wall. Thus, one can estimate an orientational trapping or escape force $F_{trap} \approx 12$ pN exerted on the particle by a magnetic orientational trap as the maximum measured repulsive force at the minimum r between the particle and wall (Fig. 4h).

Metastable periodic localization levels

The onset of repulsive interactions between gourd-shaped particles and confining walls in thick cells (Fig. 5 and 6) is similar to that in thin cells. When released from the magnetic trap while close to substrates, colloidal particles repel quickly away from the walls (initial position 1), however, a separation between them increases non-monotonically (Fig. 5 and 6). Separation vs. time curves have a step which is even more pronounced than in thin cells; this is seen in the plots as a long plateau in the dependence up to the distance ~10–15 μm away from the walls (level 2), at which particles eventually come to the rest (Fig. 5a and 6a). What is surprising and interesting is that this metastable level is far below the equilibrium sedimentation height for particles in the thick cells (Fig. 1i). Particles can reside at this metastable level without moving up or down (depending on the bottom or top substrates) due to a local potential energy minimum arising from the interplay between gravitational and elastic forces of repulsion from both substrates and particle's interactions with the cholesteric's periodic structure. However, we find from our microscopic observations that this level is only metastable. Using the low power (<10 mW) optical trap, one can assist the particle to move slightly off this metastable level 2, so that it will start moving further towards the equilibrium sedimentation height (and never back to the substrate) by itself without further assistance of the laser tweezers, slowing down when reaching the new level 3 (Fig. 5a and 6a), which is still far away from the final equilibrium sedimentation height of ~25–30 μm. Metastable levels 2 and 3 are separated by a distance roughly equal to ~p_0. Plots show that the repulsive elastic force F_w decreases non monotonically with increased separation from walls (Fig. 5c and 6c). A maximum repulsive force of ~6–7 pN was acting on the particle in its location closest to the wall (level 1), similar to the thin cells, and decreased to zero when approaching the level 2. However, there was also a sudden increase of the force to ~1 pN at the separation ~11 μm (from the top substrate) (Fig. 5c) and ~7.5 μm (from the bottom substrate) (Fig. 6c) that correspond to the small steps in the time dependencies of separation (Fig. 5a and 6a) before reaching the level 2. The repulsive force increases again to ~0.5 pN during transition between levels 2 and 3 (Fig. 5c and 6c). Positions of particles on the intermediate metastable levels 2 and 3 correspond to the potential minima arising due to the particle's interaction with the helicoidal director structure of CLC mediated by the surface anchoring on particle's surface and supplemented by the competition of F_g and elastic forces of repulsion from both substrates.

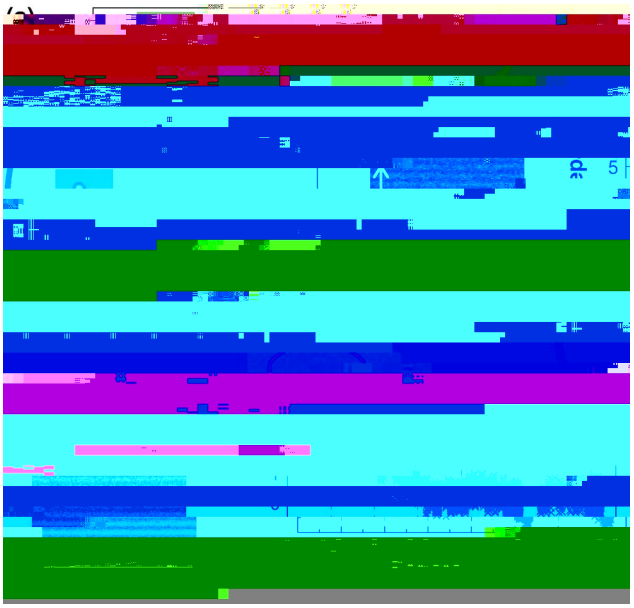

Fig. 5 Repulsive elastic interaction between a gourd-shaped particle and the top confining wall in a thick ($d \approx 60$ μm) planar cholesteric cell: (a) time dependence of separation from the wall after switching off a magnetic field. Bright field microscopy image 1 shows the orientation of particle at time $t = 0$; 3PEF-PM cross-sectional textures of a particle magnetically kept near a top substrate (b) and moving down (d) after switching off H; (c) a repulsive elastic force *vs.* separation from the top wall. Shaded area shows a moment when laser tweezers were applied to move the particle from a metastable level.

Fig. 6 Repulsive elastic interaction between a gourd-shaped particle and a bottom confining wall in a thick ($d \approx 60$ μm) planar cholesteric cell: (a) time dependence of separation from the bottom wall after switching off H; bright field microscopy images in the insets show the orientation of particle at different times indicated by arrows; 3PEF-PM cross-sectional textures of a particle magnetically trapped near a bottom substrate (b) and moving up (d) after switching off H; (c) a repulsive elastic force *vs.* separation from the bottom wall.

We fit the separation dependence of the repulsive force on the onset of elastic interactions with a power-law equation $F_w(r) \sim r^{-a}$ and find $a \approx 3$ for the repulsion from both substrates in the thin cell (Fig. 4h and k) and from the top wall in the thick cell (Fig. 5c) and $a = 5.2 \pm 0.18$ for the repulsion from the bottom wall in the thick cell (Fig. 6c). This difference in the short-range interactions can be explained by qualitatively different structure of cholesteric deformations in the narrow region between the particle and wall (compare Fig. 4a, b, 5b, and 6b).

Fig. 7 shows a time dependence of separation between a gourd-shaped particle and the bottom confining wall where the laser tweezers were used to assist displacing the particle away

metastable levels slightly decreases as the particle moves further away from the nearest confining wall, which can be seen from the orientation of the gourd-shaped particles on each such level (compare the orientation of particles in the insets 2, 3, and

each other (Fig. 9b and c). Colloidal particles sitting on the same metastable level were oriented either in the same direction or antiparallel (Fig. 9b) showing orientational ordering defined by the orientation of $\hat{\mathbf{n}}$ at the metastable level. When brought close to each other using laser tweezers, particles on different levels tended to attract to each other via elastic interactions and form colloidal structures (Fig. 9e–k) with centers of each particle's large lobe separated vertically by a distance of $\sim p_0$ (difference between levels pointed by yellow arrows 1 and 2), as determined by the use of 3PEF-PM microscopy (Fig. 9h and k). Strong bending of cholesteric layers in the vertical plane (Fig. 9h and k) prevents gourd-shaped particles from coming into direct contact with each other. Blocks of three (Fig. 9e and h) and four (Fig. 9c–k) gourd-shaped particles were assembled in the vertical plane of the cholesteric cell resulting in colloidal structures that were robust and which can be translated with laser tweezers or rotated via magnetic manipulation without breaking apart.

Conclusions

We have described the self-assembly and elastic interactions of magnetically responsive gourd-shaped colloidal particles dispersed in CLCs with a periodicity smaller than the particle's dimensions. Particles magnetically manipulated to positions near the confining walls were subsequently repelled into the bulk with a maximum elastic force of $\sim$10 pN. We demonstrated

26 C. P. Lapointe, S. Hopkins, T. G. Mason and I. I. Smalyukh, Phys. Rev. Lett., 2010, 105, 178301.
27 J. Dontabhaktuni, M. Ravnik and S. Žumer, S*oft* Matter, 2012, 8, 1657–1663.
28 B. Senyuk, Q. Liu, S. He, R. D. Kamien, R. B. Kusner, T. C. Lubensky and I. I. Smalyukh, Nature, 2013, 493, 200–205.
29 Q. Liu, B. Senyuk, M. Tasinkevych and I. I. Smalyukh, Proc. Natl. Acad. Sci. U. S. A., 2013, 110, 9231–9236.
30 M. Cavallaro Jr, M. A. Gharbi, D. A. Beller, S. Čopar, Z. Shi, R. D. Kamien, S. Yang, T. Baumgart and K. J. Stebe, S*oft* Matter, 2013, 9, 9099–9102.
31 S. Sacanna, D. J. Pine and G.-R. Yi, S*oft* Matter, 2013, 9, 8096–8106.
32 M. Zapotocky, L. Ramos, P. Poulin, T. C. Lubensky and D. A. Weitz, Science, 1999, 283, 209–212.
33 L. Ramos, M. Zapotocky, T. C. Lubensky and D. A. Weitz, Phys. Rev. E: Stat., Nonlinear, S*oft* Matter Phys., 2002, 66, 031711.
34 J. Fukuda, B. I. Lev and H. Yokoyama, Phys. Rev. E: Stat., Nonlinear, S*oft* Matter Phys., 2002, 65, 031710.
35 N. Hijnen, T. A. Wood, D. Wilson and P. S. Clegg, Langmuir, 2010, 26, 13502–13510.
36 J. S. Lintuvuori, K. Stratford, M. E. Cates and D. Marenduzzo, Phys. Rev. Lett., 2010, 105, 178302.
37 J. S. Lintuvuori, D. Marenduzzo, K. Stratford and M. E. Cates, J. Mater. Chem., 2010, 20, 10547–10552.
38 J. S. Lintuvuori, K. Stratford, M. E. Cates and D. Marenduzzo, Phys. Rev. Lett., 2011, 107, 267802.
39 R. P. Trivedi, I. I. Klevets, B. Senyuk, T. Lee and I. I. Smalyukh, Proc. Natl. Acad. Sci. U. S. A., 2012, 109, 4744–4749.
40 J. S. Evans, Y. Sun, B. Senyuk, P. Keller, V. M. Pergamenshchik, T. Lee and I. I. Smalyukh, Phys. Rev. E: Stat., Nonlinear, S*oft*,